Geophysical Journal International

Geophys. J. Int. (2009) **179,** 1361–1371 doi: 10.1111/j.1365-246X.2009.04348.x

High temperature stability of natural maghemite: a magnetic and spectroscopic study

A. U. Gehring,[1] H. Fischer,[1] M. Louvel,[2] K. Kunze[3] and P. G. Weidler[4]

[1] *Institute of Geophysics, ETH Zurich,* 8092 *Zurich, Switzerland. E-mail: agehring@ethz.ch*
[2] *Institute for Mineralogy and Petrology, ETH Zurich,* 8092 *Zurich, Switzerland*
[3] *Electron Microscopy, ETH Zurich,* 8093 *Zurich, Switzerland*
[4] *Forschungszentrum Karlsruhe, Institute for Functional Interfaces (IFG),* 76021 *Karlsruhe, Germany*

Accepted 2009 July 29. Received 2009 July 29; in original form 2009 March 18

SUMMARY

A combined magneto-mineralogical approach is used to diagnose maghemitization in magnetic grains of basaltic rock fragments from sand dunes in the Namibian desert in SW Africa. Data were obtained from static magnetic analysis, ferromagnetic resonance (FMR) spectroscopy, micro-Raman spectroscopy and electron microscopy. Micro-Raman spectroscopy showed that the magnetic grains in the lithic fragments form oxidative solid solution series with magnetite and maghemite as end-members. The five active Raman modes at 712, 665, 507, 380 and 344 cm^{-1} indicate that maghemite in the magnetic grains has well-defined structural properties. The FMR spectral analysis provides evidence for long-range dipolar coupling, which suggests intergrowth of the magnetic phases of the oxidative solid solution series. Thermomagnetic experiments and hysteresis measurements reveal a Curie temperature of about 890 K for this maghemite. Upon heating to 970 K part of the maghemite is altered to thermodynamically more stable hematite. After selective thermal decomposition of the maghemite in a protected atmosphere, the remaining magnetic phase has a Curie temperature of 850 K, characteristic for magnetite. The unique thermal stability of this natural maghemite above its Curie temperature is explained by the well-defined mineral structure, which formed during slow oxidative alteration of magnetite under arid climate conditions.

Key words: Environmental magnetism; Rock and mineral magnetism; Phase transitions; Africa.

1 INTRODUCTION

Maghemite (γ-Fe_2O_3) is a polymorph of the thermodynamically more stable hematite (α-Fe_2O_3) and has a spinel structure (AB_2O_4) similar to magnetite (Fe_3O_4). Ideal maghemite has a cation-deficient structure with a unit cell composition that can be written as $Fe_{21.33}\square_{2.66}O_{32} = 8\ Fe_{2.66}\square_{0.33}O_4 = 10.66\ Fe_2O_3$, where $\square$ stands for vacancies that occur in the B-sites. Under ambient conditions it forms by topotactic oxidation of magnetite. This oxidative process is known in the literature as maghemitization (Dunlop & Özdemir 1997). The oxidation in natural environments is generally incomplete and can lead to the coexistence of magnetite and maghemite and intermediate products denoted collectively as non-stoichiometric magnetite. Such a multimineral system is an oxidative continuous solid solution with maghemite and magnetite as end-members.

Maghemitization is a widespread process reported from different environments such as sea floor basalts, loess sediments and soils (e.g. Petersen & Vali 1987; Bina & Prévot 1989; Zhou *et al.* 2001; Chen *et al.* 2005; Fischer *et al.* 2008). In all these environments maghemitization produces a mixture of components of the oxidative solid solution series and therefore the identification of individual phases is difficult. Different magnetic parameters (e.g. saturation magnetitzation, coercivity) have been used to estimate the degree of oxidation in magnetite, but direct information about the inversion products is scarce (e.g. Zhou *et al.* 2001). The determination of the Curie temperature (T_c) as an intrinsic property of magnetic phases is commonly used for the mineralogical identification of magnetite. Without significant cation substitution this phase exhibits $T_c = 853$ K. The determination of this intrinsic parameter for maghemite is more difficult because of its metastability, that is, its strong tendency to convert into hematite at $T < 700$ K (e.g. Banin *et al.* 1993; Gehring & Hofmeister 1993; Chopra *et al.* 1999; Gendler *et al.* 2005). The few experimental data of synthetic maghemite show T_c close to 918 K (Özdemir & Banerjee 1984; Heider & Dunlop 1987; Van Oorschot & Dekkers 1999). In natural samples magnetic evidence for maghemite with a thermal stability around 870 K has been reported from basaltic rocks (e.g. Gee & Nakanishi 1995; Chévrier *et al.* 2006) and from loess sediments (e.g. Spassov *et al.* 2003).

Apart from the metastability of maghemite, its simultaneous occurrence with magnetite makes the determination of T_c for maghemite mainly in natural samples rather difficult. Low temperature magnetic measurements have been used to diagnose

maghemitization, that is, the formation of maghemite or intermediate products; in contrast to magnetite these phases exhibit no low temperature transition such as the Verwey transition. This approach, however, is not free of ambiguity because the absence of a Verwey transition can also be caused by cation substitution in magnetite (e.g. Aragón *et al.* 1985).

In recent years, thermodynamic considerations have been put forward to determine parameters controlling the stability of iron oxides/hydroxides (e.g. Tardy & Nahon 1985; Navrotsky *et al.* 2008). Navrotsky *et al.* (2008) found that particle size and hydration are main factors affecting the relative stability of polymorphic phases. They deduced thermodynamically that maghemite was stable with respect to hematite under dry conditions for grain sizes of about 16 nm. This finding is in agreement with the occurrence of maghemite in meteorites from hot deserts (e.g. Sahara) or in basaltic rocks from cold deserts of Antartica (Bland *et al.* 1998; Chévrier *et al.* 2006).

The purpose of this study is to analyse maghemitization under arid to hyperarid conditions with special focus on the stability of maghemite in a continuous solid solution with magnetite. Eolian deposits from the Namib Sand Sea in SW Africa are chosen. This sand sea is a classical dune system that has been developing since the late Pliocene (Gouldie & Eckhardt 1999). Previous studies showed that the remanent magnetization of the Namib sand is carried mainly by hematite and magnetite (Walden & White 1997; Walden *et al.* 2000). In this paper, magnetic evidence is presented which demonstrates that part of this magnetite underwent low-temperature oxidation followed by the formation of maghemite that is thermally stable above its Curie temperature. This unique property of the maghemite is discussed in context of its recent arid depositional setting.

2 SAMPLES AND METHODS

Sand samples of the Sossus formation were collected from dunes at the Sossus Vlei (24°45′21″S, 15°17′29″E) in the western central part of the Namib Sand Sea (Landcaster 1989; Schneider 2004). Bulk samples and debris separated by a commercial AlNiCo pot magnet with a lift of about 70 N (www.maurermagnetic.ch) were used. The mineral composition of the bulk and magnetic fraction was analysed by X-ray diffractrometry using a Siemens D500 with Cu Kα radiation and scintillation counter. The data were recorded between 2 and 72°2θ and 7.5 s counting time per step width of 0.03°2θ. For the microscopic analysis and the Raman spectroscopy (McMillan 1989), sections of magnetic separates mechanically polished to 1 μm grade were prepared. In addition, sections for scanning electron microscopy (SEM) were ultrapolished for 1 hr with colloidal silica particles of 25 nm in size and gently coated by carbon evaporation ($\approx$3 mm thick).

Reflectance light microscopy was performed under oil-immersion in order to analyse the ore minerals. Micro-Raman spectra of five magnetic fragments were acquired on a DILOR Labram spectrometer using a 514.5 nm Ar ion laser excitation source operating at 27.6 mW. Measurements were performed in backscattering mode under an Olympus microscope equipped with a Mitutoyo MPlan 100×/0.90 objective enabling to focus the laser spot down to 1 μm. Typical spectra were collected in 300 s with two accumulations. Data were processed using the LabSpec spectral software.

The mineral morphology and composition were characterized by SEM using an FEI Quanta200FEG instrument. Backscatter electron (BSE) images were obtained at analytical conditions of the SEM (WD 10 mm). Elemental distributions were derived from spectral mapping using an AMETEK-EDAX Genesis V system for energy dispersive X-ray (EDX) spectroscopy. Best compromise between sufficient count rates and high spectral as well as high spatial resolution was found at 10 kV high tension, 7 nA nominal beam current, 10 kcps count rate, 12.8 μs detector shaping constant, while using the build-in drift correction for life spectral mapping. Phase cluster analysis of the spectral mapping data cube was applied to highlight the major phases, based on similarity of the EDX spectra for individual pixels. Semi-quantitative element maps (concentrations in atomic per cent) were obtained by post processing using an averaging matrix of 2 × 2 pixels.

Magnetic susceptibility was measured as a function of temperature on bulk samples using an AGICO KLY-2 Kappa bridge coupled to a thermo-element in order to determine the Curie temperature of the magnetic carriers. The average heating/cooling rate was 12° min^{-1}. The Curie temperature was determined by the tangent method (Petrovský & Kapička 2006). In order to prevent oxidation, the sample was kept in a steady flow of argon during the measurements. In addition, thermal experiments in a protective atmosphere were performed in order to suppress redox reactions during heating. In this experiment the sample was put in a sealed quartz tube with argon atmosphere of about 250 mbar. The sample was heated to 923 K and maintained at this temperature for 0.5 hr before cooling to room temperature. This treatment was repeated. Susceptibility was measured before and after the thermal treatments. Furthermore, the Curie temperature of the treated sample was determined as described above.

Isothermal remanent magnetization (IRM) acquisition was measured using a Vibrating Sample Magnetometer (VSM, Princeton Measurements, Princeton, NJ, USA) in order to determine the saturation field (B_{sat}) of the ferrimagnetic phases. The applied field was increased in 10 mT steps up to 1 T. The hysteresis properties of the magnetization as a function of the magnetic field up to 1 T at room temperature and upon heating to 923 K were analysed by VSM equipped with a heating kit. The hysteresis loops were 70 per cent slope corrected for the paramagnetic constituents in the samples. In order to obtain a better insight into magnetic interactions and coercivity distribution in the solid solutions first-order reversal curves (FORC) diagrams were calculated (Pike *et al.* 2001; Roberts *et al.* 2000). The curves were recorded at room temperature before and after heating. The MATLAB routine FORCOBELLO was used to compute the FORC distribution (Winklhofer & Zimanyi 2006).

Low temperature hysteresis measurements between 12 and 300 K were performed on an alternating gradient magnetometer (Micromag 2900, Princeton Measurements) up to 1 T with field increments of 5 mT and an average acquisition time of 0.1 s. In addition, the magnetic properties of the bulk samples and separates were analysed by ferromagnetic resonance (FMR) spectroscopy. Since this method is not routinely used in rock magnetism, the basic principles are briefly summarized. The FMR spectroscopy is a special application of the classical electron spin resonance (ESR) spectroscopy, where the absorption of microwave (mw) by molecules, ions, or atoms possessing electrons with unpaired spins is measured as function of an external field (Wertz & Bolton 1972). Absorption occurs when the following resonance condition is fulfilled

$$h\nu = g\mu_B B,$$

where h is Planck's constant, ν is mw frequency, g is splitting factor, μ_B is Bohr magneton and B is external magnetic field. In contrast to ESR spectroscopy, FMR spectroscopy detects coupled spins of a magnetically ordered system, that is, the spins form a magnet with anisotropy fields. The FMR spectrum reflects the sum of all anisotropy fields and the external field, and therefore, the equation

for resonance condition has to be adapted as follows:

$$h\nu = g_{\mathrm{eff}}\mu_{\mathrm{B}}\, B_{\mathrm{eff}},$$

where g_{eff} is effective splitting factor and B_{eff} is effective field as sum of the external and internal fields.

Griscom (1980) showed that measuring FMR spectra at different frequencies provide a possibility to detect the domain state of magnetic materials. This approach was based on the assumption that the spectrum of a multidomain (MD) material with B_{eff} smaller than the saturation field (B_{sat}) is significantly different from the one with $B_{\mathrm{eff}} \geq B_{\mathrm{sat}}$. To compare the signals recorded at different frequencies the spectra are normalized by plotting the absorption versus the ratio of g_{fe}/g^*, where $g_{\mathrm{fe}} = 2$ (g-value of a free electron) and g^* is the calculated value for each magnetic field applied (B^*), that is, $g^* = h\nu/B^*\mu_{\mathrm{B}}$. Considering the resonance conditions mentioned above a g-ratio of 1 is obtained for the free electron.

In this study, the FMR spectra were recorded at room temperature by the X-band and S-band at the Laboratory of Physical Chemistry ETH Zurich. The latter was measured on a custom-built spectrometer at frequency $\nu = 4.01$ GHz, power of 2 mW and modulation amplitude of 0.1 mT. The X-band spectra at room temperature were recorded on Bruker EMX spectrometer at $\nu =$ of 9.85 GHz, power of 0.2 mW and a modulation amplitude of 1 mT. Low temperature X-band spectra were obtained from a Bruker ELESYS spectrometer using $\nu = 9.49$ GHz, power of 0.02 mW and the same modulation amplitude as in the room temperature measurements. For all spectra both the splitting factor g_{eff} and the linewidth δB were determined.

3 RESULTS AND DISCUSSION

3.1 Mineral-chemical properties

The dune sediment is in the medium sand range of grain sizes (0.25–0.5 mm). Apart from the reddish oxidized grains, which account for the colour of the dunes, dark coloured grains are macroscopically distinguishable. The dark grains can be separated magnetically from the dune sand. X-ray diffraction of these grains reveals that they are lithic fragments composed of plagioclase, clinopyroxene, and quartz. The SEM BSE images exhibit large plagioclase and clinopyroxene grains in a matrix that consists of an intergrowth of different silicate phases, which were not determined in detail. No significant mineral alteration was found for plagioclase and clinopyroxene which suggests that they were not exposed to intense weathering (Fig. 1a). Apart from the silicate BSE images suggest that the rock fragments contain Fe and Ti-rich grains with sizes up to several tens of micrometres. These grains are responsible for the magnetic properties of the rock fragments; they show a wide variety of morphologies from euhedral to skeletal forms. The latter have often dendritic and cruciform morphologies (Fig. 1b), which are indicative of quenched magnetite/titanomagnetite in basaltic rocks. Exsolution textures are often observed by which the lamellae divide the grains into angular parts varying in size. In some of the grains these parts exhibit mottling similar in shade compared to the lamellae (Fig. 2a). All these features have been reported from basaltic rocks and were interpreted as high temperature deuteric oxidation of titanomagnetite and the formation of Ti-poor magnetite and Ti-enriched phase (e.g. Price 1982). Element mapping by EDX confirms that the exsolution lamellae are enriched in Ti relative to the rest of the grain (Figs 2b and c). The exsolution pattern is also visible in the oxygen map, where Ti-rich areas posses higher atomic oxygen concentration (Fig. 2c). Considering the exsolution pattern in the basaltic rock fragments, the oxygen-enriched phase can be attributed to ferrian ilmenite formed by deuteric oxidation of a titanomagnetite precursor. Phase cluster analysis of the EDX data reveals that the mottling in the nanosize range observed in the BSE image contains of Si (along with Al, Ca) and can therefore be assigned to silicate intrusions in the exsolved Ti-poor iron oxides (Fig. 2b).

Optical microscopy reveals different ferriferous phases varying in their grades of grey colour and their isotropic or anisotropic behaviour under crossed nicols. The anisotropic phase often found in exsolution lamellae are dark greyish when examined in reflected light oil-immersion (Fig. 3a). This phase is most likely ilmenite. Hematite, as evident as anisotropic phase with white reflection occurs only as minor component. Isotropic phases exhibit a variation of greyish-tan and whitish grey colours indicative of magnetite and

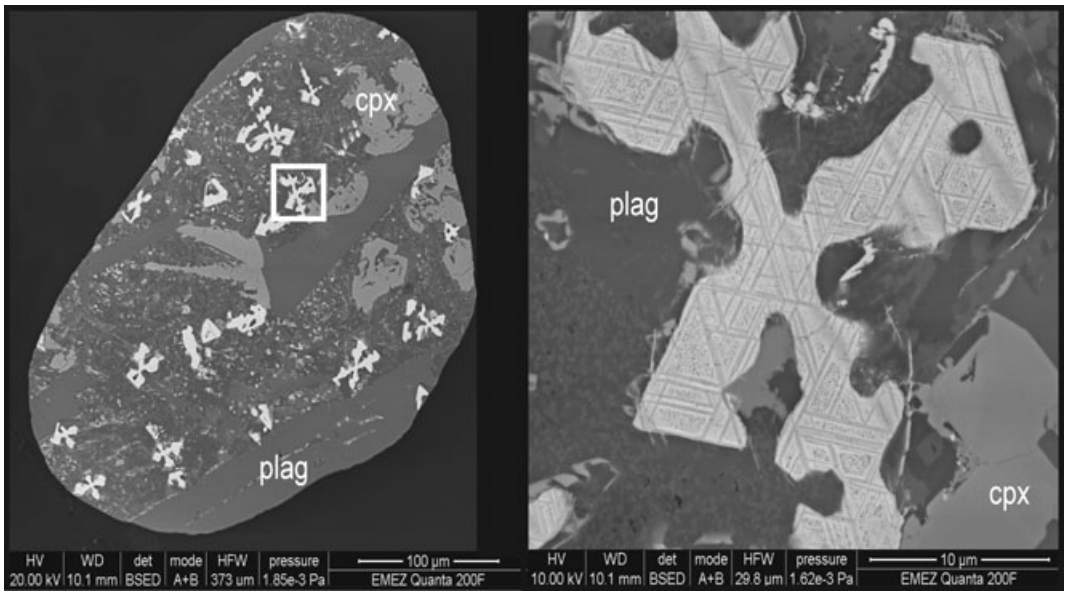

Figure 1. Backscattered electron images of basaltic fragment containing clinopyroxene (cpx), plagioclase (plag) and ferriferous grains with cruciform morphology (a); enlarged cruciform particle indicated in (a) showing exsolution features (b).

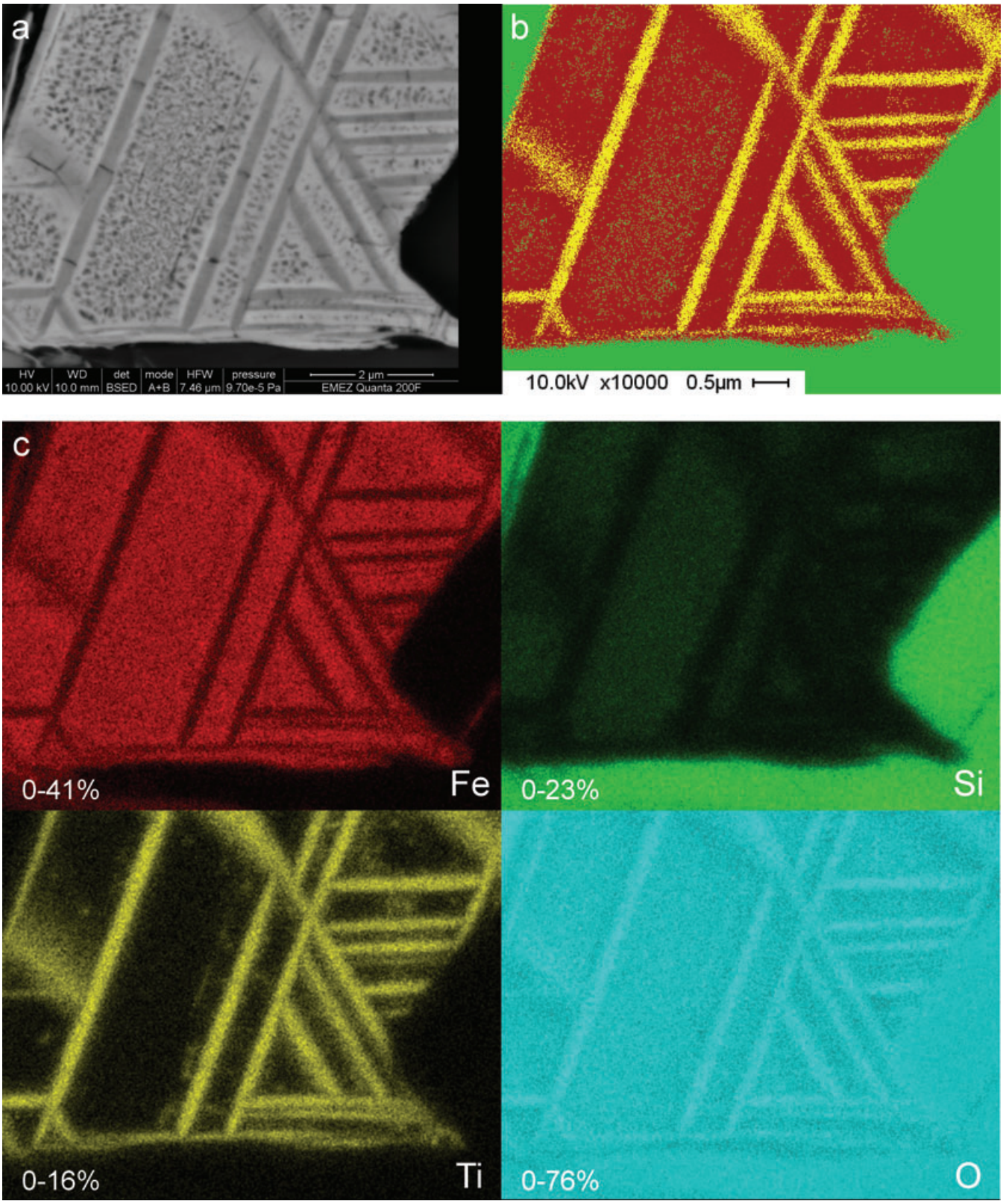

Figure 2. Backscatter electron image of an exsolution pattern in a magnetic grain (a), phase cluster analysis derived from EDX spectral mapping resulting in three major components (red: Fe-rich, yellow: Ti-rich, green: Si-rich) (b), element distributions (semi-quantitative analysis in atomic-%) for Fe, Ti, Si and O derived from same data (c).

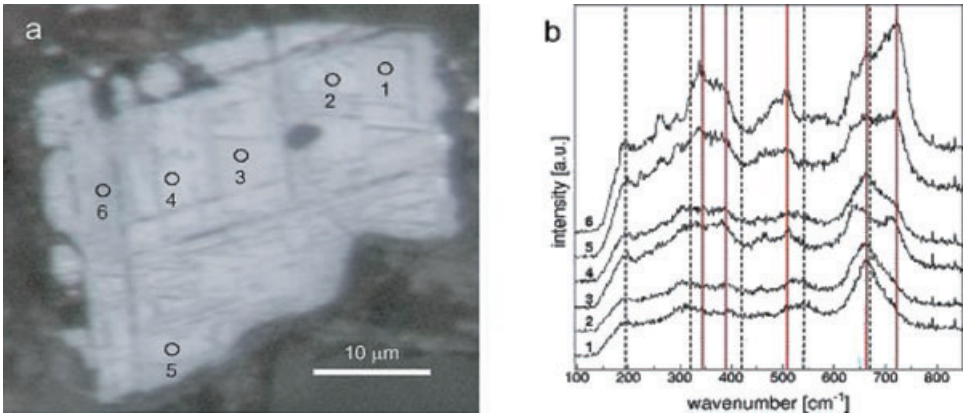

Figure 3. Reflectance light micrograph of a magnetic particle, numbers correspond to the micro-Raman analysis spots (a). Micro-Raman spectra of the indicated areas in the magnetic grain (b), the position of the active modes for magnetite (dashed lines) and maghemite (red lines) are marked. For references see text.

maghemite, respectively (Haggerty 1976). Since the two mineral phases form aggregates the optical identification of maghemite and its separation from magnetite is ambiguous. To overcome this ambiguity Raman spectroscopy was applied to the samples investigated by optical microscopy (Fig. 3b).

All spectra obtained from isotropic areas in single grains have relatively strong background due to fluorescence of iron. Moreover, they often reveal superposition of modes even in grains where the reflectance light microscopy indicates a homogeneous phase (Fig. 3). This suggests that the size of defined mineral phases is below the resolution limit of about 1μm. The spectral modes of the mineral phases are observed in the range between 150 and 1000 cm^{-1}. Several studies of vibration spectra of magnetite have been reported in the literature, and there is good agreement about the origin of the strongest modes at about 666, 538 and 306 cm^{-1}, whereas for the remaining modes between 450 and 490 cm^{-1} and at about 193 cm^{-1} the assignment is less clear (e.g. Shebanova & Lazor 2003). Modes similar to those for hematite were described for non-stoichiometric magnetite (Gupta *et al.* 2002; Shebanova & Lazor 2003; Wang *et al.* 2004). Less data are available for maghemite. Legodi & de Waal (2007) reported five Raman active modes for maghemite at about 721, 665, 507, 390 and 344 cm^{-1} (see Fig. 3b).

The above information is used for the assignment of the bands in the spectra obtained from the magnetic grains. In Fig. 3(b), the dominant bands at about 663 cm^{-1} in the spectra 1 and 2 can be attributed to symmetric stretching of Fe-O in octahedral sites and the weak bands at lower wavenumbers to Fe-O bending in magnetite (Shebanova & Lazor 2003). Spectrum 4 exhibits—in addition to the typical modes of magnetite—a shoulder at about 720 cm^{-1}. In the spectra 3, 5 and 6 this shoulder is developed as a peak and the simultaneous occurrence of peaks at 665, 507, ∼380 and 344 cm^{-1} provide clear evidence for maghemite (Legodi & de Waal 2007). Additional bands (e.g. at about 635, 292, 256 cm^{-1}), which are more pronounced in the spectra with distinct modes for maghemite, are most likely caused by non-stoichiometry of magnetite (Gupta *et al.* 2002). Taking this into account these bands reflect intermediate phases in the continuous oxidative solid solutions.

3.2 Magnetic properties

3.2.1 Susceptibility measurements

In the magnetic susceptibility-temperature measurements the heating and cooling curves of bulk samples are irreversible (Fig. 4). The

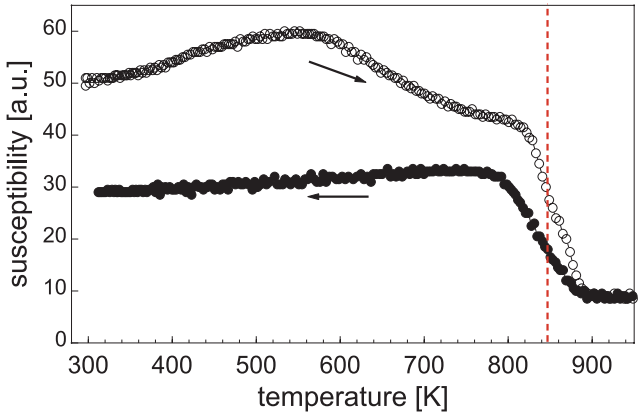

Figure 4. Heating and cooling curve of susceptibility versus temperature experiment of a bulk sample recorded in an argon atmosphere. The red dashed line indicates the Curie temperature of magnetite.

heating curve reveals two different regimes. The first one between room temperature and about 700 K is characterized by a steady increase in χ with a maximum at about 550 K followed by a gradual decrease. The second regime is associated with a drop in χ between 813 and 893 K. At higher temperature χ remains stable. Considering the Raman spectra, which suggest an intergrowth of magnetite and maghemite, the almost linear decrease reflects a superposition of the decay in magnetization near their Curie temperatures. Since magnetite has a $T_c = 853$ K, the higher $T_c \approx 890$ K can be attributed to maghemite. This value is below the experimentally determined value for synthetic pure maghemite of 918 or 933 K (Özdemir & Banerjee 1984; Fabris *et al.* 1995). By analogy to magnetite the lower value in our sample is probably due to minor Ti content in the maghemite (e.g. Dunlop & Özdemir 1997).

On cooling the increase in χ starts at 893 K and is associated with the bifurcation of the heating and cooling curves. The latter has a shallower slope than the heating curve and on further cooling below at $T \approx 793$ K a gentle decrease in χ is observed. Comparing the susceptibility at room temperature before and after the heating/cooling cycle a loss in χ of about 40 per cent during this procedure is evident (Fig. 4). The decay of χ indicates that part of the maghemite is metastable at 973 K and converts to hematite.

In order to verify this interpretation, the sample was heated in a protecting atmosphere at 1023 K, the highest reported conversion

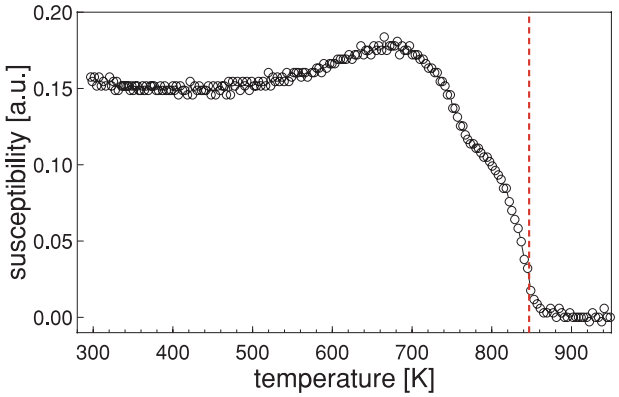

Figure 5. Susceptibility versus temperature measurement of a bulk sample in argon atmosphere after heating in a controlled atmosphere at 1023 K.

temperature of maghemite to hematite (Özdemir 1990). This treatment leads to a drop in χ to about 30 per cent of the value of the unheated sample. In further magnetic susceptibility versus temperature measurements the heating curve of the sample treated at high temperature exhibits a $T_c \approx 853$ K, which is characteristic for low-Ti magnetite (Fig. 5). Considering the Raman spectroscopic data, this finding provides clear evidence that the magnetization of the rock fragments is carried by the intergrowth of magnetite and a maghemite with $T_c \approx 890$ K.

3.2.2 FMR spectra at different frequencies

The microscopy data show that μm-size magnetic particles are subdivided into lamellar exsolutions and an emulsoid-like pattern, which are in a nanosize range. Consequently, the two frequencies approach proposed by Griscom (1980) is used to test, whether the MD state of magnetite/maghemite expected for the whole particle sizes is preserved in the exsolved areas.

In a first step the variation of the FMR signals obtained from of the dune samples is determined in order to ascertain that the samples used for the detailed investigation is representative for the dune at the site. The *X*-band spectra of bulk samples ($n = 13$) at room temperature exhibits a broad near symmetric signal with $g_{\text{eff}} = 2.22 \pm 0.03$ and linewidth (δB) of 158 ± 8 mT characteristic for both magnetite and maghemite. (e.g. Griscom 1984; Gehring *et al.* 1990). The comparison of spectra yielded from the bulk and the separates reveals no significant difference, which indicates the FMR signals originate from the ferrimagnetic phases magnetite and maghemite in the rock fragments. The spectral parameters of the separate used for the multifrequency measurements was $\delta B = 161$ mT, and $g_{\text{eff}} = 2.22$ corresponding to $B_{\text{eff}} = 0.316$ T (Fig. 6a). The comparison of B_{eff} with $B_{\text{sat}} = 0.3$ mT obtained from IRM measurements suggests that the absorption peak is associated with saturation of the ferrimagnetic material.

The spectrum recorded at *S*-band is asymmetric with $\delta B = 130$ mT. The g_{eff} value is 3.49, which corresponds to a B_{eff} of 80 mT. Considering B_{sat} deduced from IRM data the maximum absorption in the *S*-band spectrum occurs in a field where the magnetite/maghemite is far from saturation.

The comparison of the two spectra by normalizing their *g*-ratios to that of a free electron, as proposed by Griscom (1980), shows for the *X*-band a near symmetric absorption close to 1, whereas for the *S* band a broader asymmetric absorption is observed (Fig. 6b). Since it is well known that domain walls have a strong effect on the FMR absorption properties (Polder & Smit 1953) the observed spectral difference can be explained by the domain state of the material. At the absorption peak in the *X*-band measurements the magnetite/maghemite is saturated, that is, the material reflects a single domain state. In contrast, in the *S*-band the maximum absorption occurs where domain walls still exist and therefore they are affected by the microwave radiation. This effect can explain the asymmetry of the absorption spectrum and its significant departure from the normalized *g*-ratio of 1 (Fig. 6b). Following this argumentation the FMR data clearly indicates magnetite/maghemite in MD states.

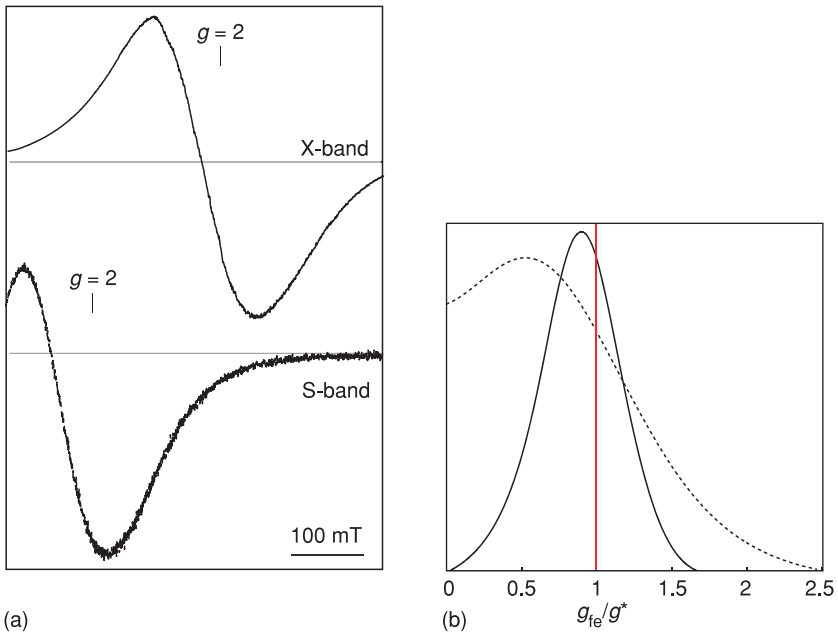

Figure 6. (a) First derivative of *X*- and *S*-band FMR absorption spectra of a bulk sample. (b) Comparison of the *X*-band (solid line) and *S*-band (dashed line) absorption spectra by their normalized resonance fields as proposed by Griscom (1980). The red line indicates the *g*-ratio for a free electron. For further explanation see text.

3.2.3 Hysteresis properties

Hysteresis plots at room temperature of five bulk samples and five magnetic separates exhibit a low coercivity phase with a saturation field (B_{sat}) of 0.3 T (Fig. 7a). No significant difference between the hysteretic parameters of the two sample sets is found. Considering all samples the coercivity B_c is 16.2 $\pm$ 0.8 mT and the squarness ratio m_r/m_s is 0.21 $\pm$ 0.01. The similarity of the hysteresis properties for all samples suggests that the remanent magnetization of the dune samples is dominated by magnetite and maghemite in the rock fragments. The contribution of the ferric oxides of the grain coatings, which account for the reddish colour of the dunes is negligible.

The FORC diagrams corresponding to the hysteresis plots at room temperature exhibit two contrasting features (Fig. 7b). One spreads along B_b with $B_c < 5$ mT while the other show an open contours slightly diverging from the $B_b = 0$ axes. Such features

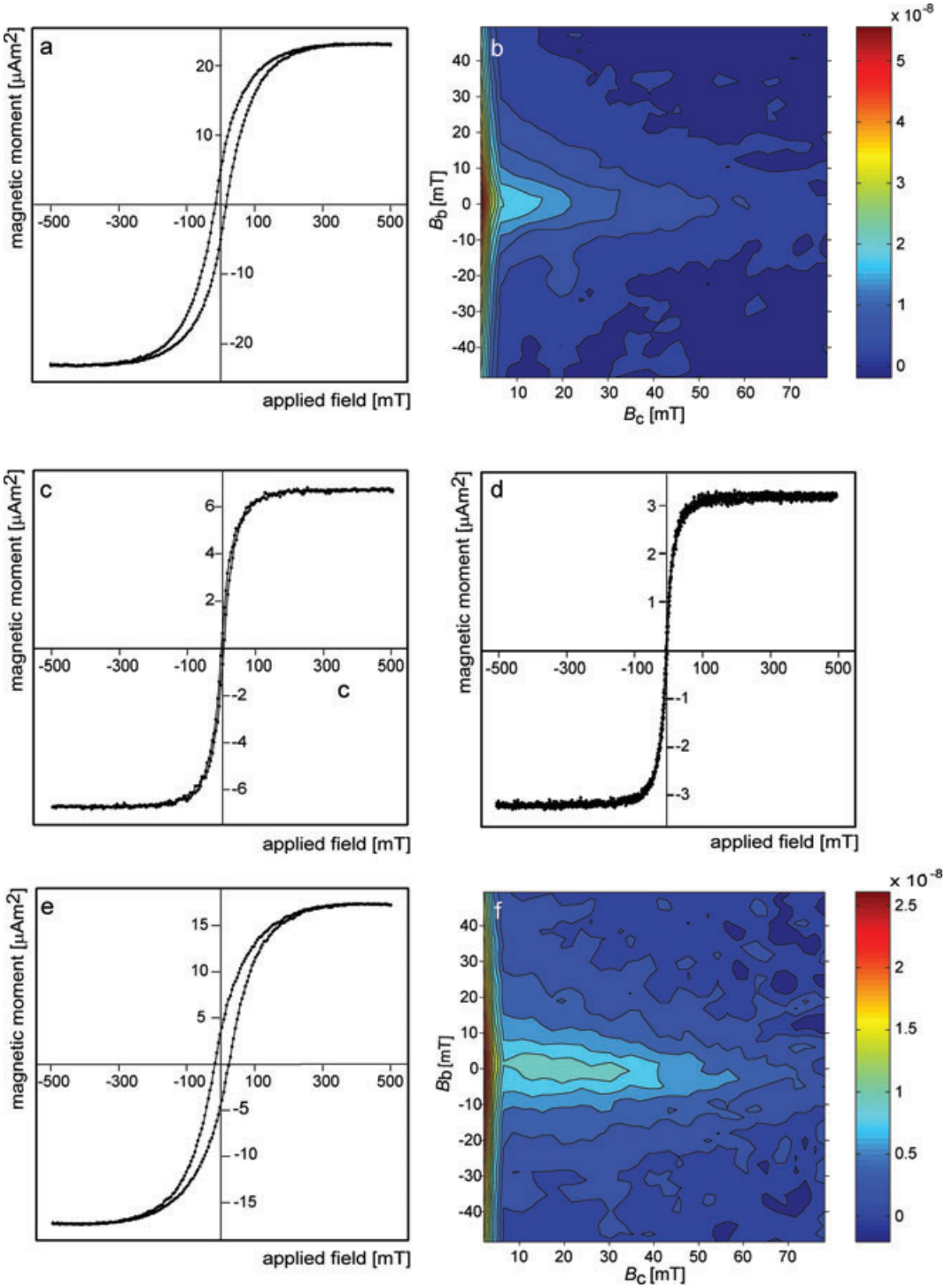

Figure 7. Magnetic moment versus applied field plot (a) and FORC diagram (b) of basaltic fragments at room temperature; hysteresis loops measured at 853 K (c) and at 893 K (d), and hysteresis curve (e) and FORC diagram (f) of the sample at room temperature after heating. The hysteresis loops were 70 per cent slope corrected for the paramagnetic contribution and the FORC diagrams were processed without reversible ridge analysis.

Table 1. Hysteresis parameters of basaltic rock fragments upon heating to 893 K and subsequent cooling to room temperature.

T (K)	B_c (mT)	m_r (μAm^2)	m_s (μAm^2)	m_r/m_s
298	15.8	5.04	23.06	0.22
573	7.1	2.69	19.25	0.14
673	7.1	2.15	14.71	0.15
773	5.8	1.41	10.29	0.14
823	4.6	1.06	8.31	0.13
853	3.4	0.67	6.71	0.10
873	2.5	0.53	4.67	0.11
893	2.2	0.33	3.21	0.10
Cooling				
893	2.0	0.35	2.86	0.12
873	2.7	0.55	4.57	0.12
853	3.2	0.64	6.07	0.14
823	4.7	0.99	7.66	0.16
773	6.1	1.29	9.67	0.17
573	11.4	2.49	14.19	0.26
473	14.6	3.00	15.40	0.21
373	18.1	3.50	16.57	0.23
301	20.4	3.90	17.17	0.24

Table 2. Hysteresis parameters and FMR spectral parameters of basaltic rock fragments at low temperatures.

T (K)	B_c (mT)	m_r (μAm^2)	m_s (μAm^2)	m_r/m_s	δB (mT)	g_{eff}
290	19.5	0.87	4.99	0.17	168	2.26
270	20.5	0.89	5.00	0.18		
250	21.8	0.90	4.94	0.18		
210	28.7	0.93	3.64	0.26		
200					172	2.34
190	30.3	0.96	3.66	0.26		
170	31.7	0.98	3.65	0.27		
150	32.7	1.01	3.86	0.26	211	2.43
130	34.9	1.01	3.41	0.30	204	2.44
120	35.3	1.02	3.42	0.30	205	2.44
110	35.8	1.03	3.46	0.30	205	2.44
100	36.7	1.03	3.4	0.30	201	2.47
90	36.8	1.04	3.44	0.30		
80	37.2	1.05	3.44	0.31	203	2.52
70	37.6	1.06	3.43	0.31		
60					199	2.54
50	38.7	1.09	3.47	0.31		
30	42.2	1.16	3.51	0.33		
12	48.0	1.23	3.49	0.35	172	2.57

are attributed to two grain size populations. The spread along $B_c <$ 5 mT has been observed for ferrimagnetic materials in a MD or a superparamagnetic (SP) state (Pike *et al.* 2001; Brem *et al.* 2006). Considering the FMR data a SP state can be ruled out. The second feature with the open contour was described for ferrimagnetic materials in a pseudo-single domain state (e.g. Roberts *et al.* 2000). The density distribution of the coercivities as expressed by the scale bar suggests a prevalence of the feature with the lower coercivity. Different B_c populations in MD magnetite grains have been explained by stress arising from lattice mismatch caused by shrinking of the unit cell during oxidation (Cui *et al.* 1994). Moreover increasing oxidation can lead to fracturing and subsequently to smaller grain sizes, that is, increased B_c. With this in mind the two B_c populations can be interpreted as extrinsic effect of the magnetite due to oxidation.

For the hysteresis measurements of heated magnetic separates, the chosen temperatures are adapted to the different regimes in the susceptibility measurements (Table 1). Between room temperature and 573 K (maximum in χ), B_c decreases by a factor 2 and also the squareness ratio experiences a significant reduction. The simultaneous magnetic softening, that is, decrease in B_c, and increase in χ can be explained by the elimination effect of stacking faults in intergrown magnetite and maghemite (Banfield *et al.* 1994). Moreover this decrease in B_c suggests that the two ferrimagnetic phases with nearly compatible lattices are magnetically coupled. Upon further heating B_c remains stable up to 673 K above, which it decreases steadily. At 853 K B_c has a value of 3.4 mT. The hysteretic properties persist up to 893 K where $B_c = 2.2$ mT was measured (Table 1). A similar decrease in B_c was reported for magnetite and maghemite (Dunlop 1987; Özdemir 1990). In contrast to the coercivity, the squareness ratio exhibits only minor changes at $T >$ 573 K (Table 1). The comparison of the untreated and heated sample at room temperature shows no reversibility with respect to B_c, m_r and m_s. The magnetic moments decreases by about a fourth during the heat treatment (Table 1).

The occurrence of low-coercivity hysteretic behaviour at $T >$ 853 K agrees well with the susceptibility–temperature curves and provides additional evidence for maghemite with high temperature stability (Figs 7c and d). The decrease in m_r and the increase in B_c after heating suggests that part of the maghemite is metastable at 973 K and converts into hematite (Fig. 7e; Table 1). After heating the FORC plot at room temperature exhibits two features. The feature with $B_c <$ 5 mT is similar to the one in the untreated samples (Fig. 7f). The other feature with $B_c >$ 5 mT is characterized by a converging inner contour which is almost closed. Features with closed contours are indicative of single domain ferrimagnetic materials. Moreover a change in the density distribution of the coercivity is observed by comparison of the FORC plots before and after heating. After the thermal treatment the relative contribution of the population with $B_c >$ 5 mT increases (Fig. 7f). Following the above argumentation the changes in the hysteretic parameters after the thermal treatment are most likely due to fracturing of MD-sized particles caused by the alteration of maghemite.

3.3 Low temperature properties

3.3.1 Coercivity and squareness ratio

Since magnetite and maghemite exhibit different behaviour at low temperature, hysteresis measurements between room temperature and 12 K could be used to discriminate the two phases. The low temperature behaviour of magnetite is more complicated because of the temperature dependence of the magnetocrystalline constant *K1*, which changes sign at the isotropic point around 135 K (Bickford 1950). Moreover stoichiometric magnetite undergoes a phase transition at about 120 K. This transition is associated with a significant increase in B_c and in the squareness ratio (Dunlop & Özdemir 1997). In contrast maghemite exhibits gradual increase in B_c upon cooling as shown by Morrish & Watt (1958).

The B_c of the dune sand increases with decreasing *T*. A more prominent increase is found between 250 and 210 K and at $T <$ 50 K (Table 2). The squareness ratio increases as T decreases, and the ratio of 0.17 at room temperature is about half of that at 12 K. Neither parameters exhibit any indication of a Verwey transition as might be expected for stoichiometric magnetite. It is well known that departure from stoichiometry can suppress this transition (e.g. Dunlop & Özdemir 1997) and that maghemite exhibits no low temperature transition (Morrish & Watt 1958). With this in mind, the observed hysteresis behaviour at low temperature suggests

that the magnetic grains in the basaltic fragments mainly consist of maghemite and non-stoichiometric magnetite.

3.3.2 FMR behaviour

At 290 K the *X*-band spectrum of the sample used for the low temperature FMR experiment has $g_{\text{eff}} = 2.26$ and $\delta B = 168$ mT. Upon cooling the line width δB strongly increases by about 40 mT between 200 and 150 K, followed by minor narrowing to 60 K and by prominent narrowing of 25 mT at 16 K. The g_{eff}-values show a general increase down to 16 K with a plateau-like range between 150 and 110 K.

Compared to hysteresis data, low temperature FMR data of polycrystalline stable single domain or MD magnetite and maghemite have been rarely reported (e.g. Sharma & Waldner 1977; Gehring *et al.* 1990). Generally an increase in g_{eff} and δB is found upon cooling for these ferrimagnetic phases (e.g. Friebele *et al.* 1974; Gehring *et al.* 1990; Stankowski *et al.* 2006; Fischer *et al.* 2007). The dune sample exhibits the expected shift of g_{eff} to higher fields, which indicates that the internal field in the samples increases. This behaviour can be explained by a growth of the anisotropy field (e.g. Schlömann & Zeender 1958; Griscom 1984). Such growth should also be reflected in a spectral broadening, that is, increase in δB. The dune sample, however, shows a general trend to lower δB at $T < 150$ K, which is more prominent below 60 K (Table 2). The different behaviour of δB and g_{eff} suggests that the spectral parameters cannot be explained solely by increasing anisotropy. Geschwind & Clogston (1957) suggested that the narrowing in heterogeneous ferromagnetic materials can be an effect of long-range dipolar interactions. These authors argued that dipolar coupling can even out heterogeneity of absorption in the material, that is, a more common resonant frequency is yielded. With this in mind, such a process could explain the narrowing in our sample with its heterogeneous mineral-chemical composition. The most pronounced decrease in δB occurs at $T < 60$ K, where ilmenite has its Néel temperature, T_{N}. Since this mineral phase is associated with magnetite and maghemite in the rock fragments, it is plausible to argue that the magnetic ordering of ilmenite further changes the dipole interactions in the sample.

3.4 Stabilization of maghemite

The mineral composition and texture of the lithic fragments as well as the dentritic morphology of the magnetic components are indicative of a basaltic source rock. Jurassic Karoo flood basalt, which covered major part of southern Africa can be considered as the most likely source for these lithic fragments (e.g. Rehfeldt *et al.* 2007). Since no maghemite was found in the remains of the Karoo flood basalt (Kosterov 2001), it is feasible to assume that this mineral phase is formed during low temperature oxidation under arid climate conditions. The assumption of such conditions is supported by the fact that silicates of basaltic grains reveal no significant indication of chemical weathering. Moreover, the occurrence of maghemite in the desert environment agrees well with thermodynamic considerations by Navrotsky *et al.* (2008), which show that dry conditions can increase the stability of maghemite with respect to its polymorph hematite.

The simultaneous occurrence of magnetite and maghemite and probably of non-stoichiometric intermediate phases, hints at an oxidation process caused by solid-state diffusion. Compared to an ideal spinel structure, maghemite has a concentration of defects of one ninth with respect to the cation sites, that is, B-sites. Therefore, it was postulated that the diffusion of Fe atoms via defects and the simultaneous oxidation of Fe(II) to Fe(III) at B-sites, because of local charge neutrality, is the determinant reaction step during maghemitization (e.g. Freer & O'Reilly 1980). Studies on mid-ocean ridge basalts suggest that such a process takes place over millions of years (e.g. Freer & O'Reilly 1980; Zhou *et al.* 2001), and,, therefore, a relatively low diffusion rate can be supposed. Slow diffusion together with low chemical weathering rates characteristic for arid environments can be an explanation for the presence of a magnetically well-defined maghemite in the basaltic rock fragments. This is supported by the finding that the degree of maghemitization is inhomogeneous in the magnetite grains and no enhanced oxidation at the grain surfaces is observed. Since different blocks of magnetite separated by ilmenite lamellae reveal different proportions of maghemite, it is likely that heterogeneities (e.g. subgrain-boundaries, dislocations) in the magnetite inherited from exsolution processes affects diffusion and formation of maghemite during weathering.

4 CONCLUSIONS

Basaltic rock fragments deposited in dunes in the Namib Sand Sea formed since late Pliocene contain magnetic grains, which consist of an oxidative solid solution series with magnetite and maghemite as end-members. Magnetite occurs in blocks separated by ilmenite-like lamellae and reveals different degrees of maghemitization. Maghemite, as an oxidation product of magnetite exhibits thermal stability at temperatures above its Curie temperature of about 890 K. The unique thermal stability for natural maghemite is explained by its well-defined structure formed during slow chemical weathering under arid climate conditions.

ACKNOWLEDGMENTS

The authors are grateful to Inès Gracia Rubio (Laboratory of Physical Chemistry ETH Zurich) for her support in the *X*- and *S*-band measurements, L. Fontboté (Université de Genève) for his help with the reflectance light microscopy, and Bill Lowrie for this critical review of the manuscript. Part of this work was supported by ETH research grant TH02296.

REFERENCES

Aragón, R., Buttrey, D.J., Shepherd, J.P. & Honig, J.M., 1985. Influence of nonstoichiometry on the Verwey transition, *Phys. Rev B.,* **31,** 430–436.

Banfield, J.F., Wasilewski, P.J. & Veblen, D.R., 1994. TEM study of the relationships between the microstructures and magnetic properties of strongly magnetized magnetite and maghemite, *Am. Min.,* **79,** 654–667.

Banin, A., Ben-Shlomo, T., Margulies, L., Blake, D.F., Mancinelli, L. & Gehring, A.U., 1993. The nanophase iron mineral(s) in Mars soil, *J. geophys. Res.,* **98,** 20831–20853.

Bickford, L.R., 1950. Ferromagnetic resonance absorption in magnetite single crystals, *Phys. Rev.,* **78,** 449–547.

Bina, M. & Prévot, M., 1989. Thermomagnetic investigation of titanomagnetite in submarine basalts: evidence for differential maghemitization, *Phys. Earth planet. Inter.,* **54,** 169–179.

Bland, P.A. *et al*., 1998. Climate and rock weathering: a study of terrestrial age dated ordinary chondritic meterorites from hot desert regions, *Geochim. Cosmochim. Acta,* **62,** 3169–3184.

Brem, F., Tiefenauer, L., Fink, A., Dobson, J. & Hirt, A.M., 2006. A mixture of ferritin and magnetite nanoparticles mimics the magnetic properties of human brain tissue, *Phys. Rev. B,* **73,** 224427-1–224427-5.

Chen, T., Xu, H., Xie, Q., Chen, J., Ji, J. & Lu, H., 2005. Characteristics and genesis of maghemite in Chinese loess and paleosols: mechanism for magnetic susceptibility enhancement in paleosols, *Earth planet. Sci. Lett.,* **240,** 790–802.

Chévrier, V., Mathé, P.-E., Rochette, P. & Gunnlaugsson, H.P., 2006. Magnetic study of an Antarctica weathering profile on basalt: implications for recent weathering on Mars, *Earth planet. Sci. Lett.,* **244,** 501–514.

Chopra, G.S., Real, C., Alcalá, M.D., Pérez-Maqueda, L.A., Subrt, J. & Criado, J.M., 1999. Factor influencing the texture and stability of maghemite obtained from thermal decomposition of lepidocrocite, *Chem. Mater.,* **11,** 1128–1137.

Cui, Y., Verosub, K.L. & Roberts, A.P., 1994. The effect of low-temperature oxidation on large multi-domain magnetite, *Geophys. Res. Lett.,* **21,** 757–760.

Dunlop, D. & Özdemir, Ö., 1997. *Rock Magnetism: Fundamentals and Frontiers,* Cambridge University Press, Cambridge, UK.

Dunlop, D.J., 1987. Temperature dependence of hysteresis in 0.04–0.22 μm magnetite and implication for domain structure, *Phys. Earth planet. Inter.,* **46,** 100–119.

Fabris, J.D., Coey, J.M.D., Qinian, Qi & Mussel, W.N., 1995. Characterization of Mg-rich maghemite from tuffite, *Am. Min.,* **80,** 664–669.

Fischer, H., Luster, J. & Gehring, A.U., 2007. EPR evidence for maghemitization of magnetite in a tropical soil, *Geophys. J. Int.,* **169,** 909–916.

Fischer, H., Luster, J. & Gehring, A.U., 2008. Magnetite weathering in a Vertisol with seasonal redox-dynamics, *Geoderma,* **143,** 41–48.

Freer, R. & O'Reilly, W., 1980. The diffusion of Fe^{2+} ions in spinels with relevance to the process of maghemitization, *Min. Mag.,* **43,** 889–899.

Friebele, E.J., Griscom, D.L., Marquardt, C.L., Weeks, R.A. & Prestel, D., 1974. Temperature dependence of the ferromagnetic resonance linewidth of lunar soils, iron and magnetite precipitates in simulated lunar glasses, and nonspherical metallic iron particles, in *Proceedings of the Fifth Lunar Sci. Conference, Geochim. Cosmochim. Acta,* **3** (Suppl. 5), 2729–2736.

Gee, J. & Nakanishi, M., 1995. Magnetic petrology and magnetic properties of western Pasific guyots: implications for seamount paleopoles, *Proc. ODP Sci. Results,* **144,** 615–630.

Gehring, A.U. & Hofmeister, A.M., 1993. The transformation of lepidocrocite during heating—a magnetic and spectroscopic study, *Clays Clay Min.,* **42,** 409–415.

Gehring, A.U., Karthein, R. & Reller, A., 1990. Activated state in the lepidocrocite structure during thermal treatment, *Naturw.,* **77,** 177–179.

Gendler, T.S., Shcherbakov, V.P., Dekkers, M.J., Gapeev, A.K., Gribov, S.K. & McClelland, M., 2005. The lepidocrocite-maghemite reaction chain—I. Aquisition of chemical remanent magnetization by maghemite, its magnetic properties and thermal stability, *Geophys. J. Int.,* **160,** 815–832.

Geschwind, S. & Clogston, A.M., 1957. Narrowing effect of dipole force on inhomogeneously broadened lines, *Phys. Rev.,* **108,** 59–63.

Gouldie, A.S. & Eckhardt, F., 1999. The evolution of the morphological framework of the central Namib desert, Namibia, since the early Cretaceous, *Geogr. Ann.,* **81A**(3), 443–458.

Griscom, D.L., 1980. Ferromagnetic resonance of fine-grained precipitates in glass—a thumbnail review, *Non-Cryst. Solids,* **42,** 287–296.

Griscom, D.L., 1984. Ferromagnetic resonance of precipitated phases in natural glasses, *J. Non-Cryst. Solids,* **67,** 81–118.

Gupta, R., Sood, A.K., Metcalf, P. & Honig, J.M., 2002. Raman study of stoichiometric and Zn-doped Fe_3O_4, *Phys. Rev. B,* **65,** 104430.

Haggerty, S.E., 1976. Oxidation of opaque oxides in basalts, in Oxide minerals, in *Short course Notes,* **Vol. 3**, pp. 1–20, ed. Rumble, D. III, Mineralogical Society of America.

Heider, F. & Dunlop, D.J., 1987. Two types of chemical remanent magnetization during the oxidation of magnetite, *Phys. Earth planet. Inter.,* **46,** 24–45.

Kosterov, A., 2001. Magnetic properties of subaerial basalts at low temperatures, *Earth Planets Space,* **53,** 883–892.

Lancaster, N., 1989. *The Namib Sand Sea: Dune Forms, Processes, and Sediments,* Balkema, Rotterdam.

Legodi, M.A. & De Waal, D., 2007. The preparation of magnetite, goethite, hematite and maghemite of pigment quality from mill scale iron waste, *Dyes and Pigments,* **74,** 161–168.

McMillan, P.F., 1989. Raman spectroscopy in mineralogy and geochemistry, *Ann. Rev. Earth planet. Sci.,* **17,** 255–283.

Morrish, A.H. & Watt, L.A.K., 1958. Coercive force of iron oxide micropowders at low temperature, *J. appl. Phys.,* **29,** 1029–1033.

Navrotsky, A., Mazeina, L. & Majzlan, J., 2008. Size-driven structural and thermodynamic complexity in iron oxides, *Science,* **319,** 1635–1638.

Özdemir, Ö., 1990. High-temperature hysteresis and thermoremanence of single-domain maghemite, *Phys. Earth planet. Inter.,* **65,** 125–136.

Özdemir, Ö. & Banerjee, S.K., 1984. High temperature stability of maghemite (γ-Fe2O3), *Geophys. Res. Lett.,* **11,** 161–164.

Petersen, N. & Vali, H., 1987. Observation of shrinkage cracks in ocean floor titanomagnetites, *Phys. Earth planet. Inter.,* **46,** 179–205.

Petrovský, E. & Kapička, A., 2006. On determination of the Curie point from thermomagnetic curves, *J. geophys. Res.,* **111,** B12S27, doi:10.1029/2006JB004507.

Pike, C.R., Roberts, A.P., Dekkers, M.J. & Verosub, K.L., 2001. An investigation of multi-domain hysteresis mechanisms using FORC diagrams, *Phys. Earth planet. Inter.,* **126,** 11–25.

Polder, D. & Smit, J., 1953. Resonance phenomena in ferrites, *Rev. Mod. Phys.,* **25,** 89–90.

Price, G.D., 1982. Exsolution in titanomagnetite as indicator of cooling rates, *Min. Mag.,* **46,** 19–25.

Rehfeldt, T., Jakob, D.E., Carlson, R.W. & Foley, S.F., 2007. Fe-rich dunite xenoliths from South African kimberlites: cumulates from Karoo flood basalts, *J. Petrol.,* **48,** 1–23.

Roberts, A.P., Pike, C.R. & Verosub, K.L., 2000. First-order reversal curve diagrams: a new tool for characterizing the magnetic properties of natural samples, *J. geophys. Res.,* **105,** 28461–28475.

Schlömann, E. & Zeender, J.R., 1958. Ferromagnetic resonance in polycrystalline nickel ferrite aluminate, *J. appl. Phys.,* **29,** 341–343.

Schneider, G., 2004. *The Roadside Geology of Namibia,* Gebrüder Borntraeger, Berlin.

Sharma, V.K. & Waldner, F., 1977. Superparamagnetic and ferrimagnetic resonance of ultrafine Fe3O4 particles in ferrofluids, *J. appl. Phys.,* **48,** 4298–4302.

Shebanova, O.N. & Lazor, P., 2003. Raman spectroscopic study of magnetite (FeFe2O4): a new assignment for the vibrational spectrum, *J. Solid State Chem.,* **174,** 424–430.

Spassov, S., Heller, F., Kretzschmar, R., Evans, M.E., Yue, L.P. & Nourgaliev, D.K., 2003. Detrital and pedogenic magnetic mineral phases in the loess/paleosol sequence at Lingtai (Ventral Chinese Loess Plateau), *Phys. Earth planet. Inter.,* **140,** 255–275.

Stankowski, J., Kempiński, Łos, S., Bednarski, W., Waplak, S. & Micnas, R., 2006. Two paramagnetic iron states at the Verwey phase transition in magnetite, *J. Magn. Magn. Mater.,* **301,** 88–93.

Tardy, Y. & Nahon, D., 1985. Geochemistry of laterites, stability of Al-goethite, Al-hematite, and Fe^{3+}-kaolinite in bauxites and ferricretes – an approach to the mechanism of concretion formation, *Am. J. Sci.,* **285,** 865–903.

van Oorschot, I.H.M. & Dekkers, M.J., 1999. Dissolution behaviour of fine-grained magnetite and maghemite in the citrate–bicarbonate–dithionite extraction method, *Earth planet. Sci. Lett.,* **167,** 283–295.

Walden, J. & White, K.H., 1997. Investigation of the controls on dune colour in the Namib Sand Sea mineral magnetic analyses, *Earth planet. Sci. Lett.,* **152,** 1987–201.

Walden, J., White, K.H., Kilcoyne, S.H. & Bentley, P.M., 2000. Analysis of iron oxide assemblage within Namib dune sediments using high field remanence measurements (9T) and Mössbauer analysis, *J. Quart. Sci.,* **15,** 185–195.

Wang, A., Kuebler, K.E., Jolliff, B.L. & Haskin, L.A, 2004. Raman spectroscopy of Fe-Ti-Cr-oxides, case study: Martian meteorite EETA 79001, *Am. Miner.,* **89,** 665–680.

Wertz, J.E. & Bolton, J.R., 1972. *Electron Spin Resonance,* McGraw-Hill, New York.

Winklhofer, M. & Zimanyi, T., 2006. Extracting the intrinsic switching field distribution in perpendicular media: a comparative analysis, *J. appl. Phys.,* **99,** 08E710.

Zhou, W., Van Der Voo, R., Peacor, D.R., Wang, D. & Zhang, Y., 2001. Low-temperature oxidation in MORB of titanomagnetite to titanomaghemite: a gradual process with implications for marine magnetic anomaly amplitudes, *J. geophys. Res.,* **106,** 6409–6421.